# NMR investigation of multi-scale dynamics in ionic liquids containing Li+ and La3+: From vehicular to hopping transport mechanism

Ousmane Karé, Antonio de Souza Braga Neto, Baptiste Rigaud, Quentin Berrod, Sandrine Lyonnard, Clément Cousin, Juliette Sirieix-Plénet, Anne-Laure Rollet, Guillaume Mériguet

Journal of Ionic Liquids 4 (2024) 100087

Contents lists available at ScienceDirect

Journal of Ionic Liquids

journal homepage: www.elsevier.com/locate/jil

# NMR investigation of multi-scale dynamics in ionic liquids containing $Li^+$ and $La^{3+}$ : From vehicular to hopping transport mechanism

Ousmane Karé [a], Antonio De Souza Braga Neto [a], Baptiste Rigaud [b], Quentin Berrod [c], Sandrine Lyonnard [c], Clément Cousin [a], Juliette Sirieix-Plénet [a], Anne-Laure Rollet [a,*], Guillaume Mériguet [a,*]

[a] Sorbonne Université/CNRS, Laboratoire Physico-Chimie des Électrolytes et Nano-Systèmes Interfaciaux (PHENIX), 4 place Jussieu, Paris, France
[b] Sorbonne Université, Fédération de Chimie et Matériaux de Paris Centre (FCMAT), 4 Place Jussieu, Paris, France
[c] Université Grenoble Alpes, CNRS, CEA, IRIG-SyMMES, 17 avenue des Martyrs, Grenoble, France

ARTICLE INFO

*Keywords:*
Ionic liquid
Electrolyte
Diffusion
NMR relaxation
Fast field cycling relaxometry
Solvation
Lithium
Lanthanum

ABSTRACT

The dynamics in mixtures of ionic liquid and monoatomic cations has been studied at different time scales ranging from the nanosecond up to the second. The mixtures were composed of cholinium bis(trifluoromethanesulfonyl)imide ([Chol][TFSI]) and LiTFSI, with LiTFSI mole fraction, $x_{LiTFSI}$, spanning from 0 to 0.5 (saturated solution), and [Chol][TFSI] and $La(TFSI)_3$ from 0 to 0.12. The translational self-diffusion coefficients of $Chol^+$, $TFSI^-$ and $Li^+$ have been measured, along with NMR their relaxation times at various magnetic fields, in order to decipher the intertwined dynamics between the ions, and to reveal how the local dynamics impact the long range translational diffusion. When the concentrations of lithium and lanthanum are increased in the liquid, the long range dynamics of all the ions drop. In the case of LiTFSI, the self-diffusion coefficient of lithium becomes higher than the one of TFSI at high concentration, revealing a change in lithium transport mechanisms. The NMR relaxation data confirm this change, showing a clearer transition at $x_{LiTFSI} = 0.15$. It is interpreted as a change from a vehicular transport mechanism of the lithium below $x_{LiTFSI} = 0.15$ to a hopping mechanism above. A similar crossover seems to occur in the lanthanum solutions. This phenomenon seems correlated to the departure of the hydroxyl group of the organic cation from the lithium solvation shell.

## 1. Introduction

Ionic liquids (IL) are fascinating liquids that exhibit remarkable structural diversity leading to a surge in various fields such as organic synthesis, metal or biomolecules extractions, electrochemistry, catalysis . . . (Greer et al., 2020). Their specificity originates from a delicate balance between interactions: Coulombic, steric, Van der Waals, H-bond, $\pi - \pi$, etc. (Hayes et al., 2015). When a new species is introduced in the system, the above-mentioned balance can be strongly altered and the consequences for the applications for which ionic liquids are designed, can be very important. Hence, the identification and understanding of the changes of all the properties of the IL has to be carried out. Both the structural and dynamical properties are modified upon the addition of a supplementary species. For instance, in the frequently studied IL, 1-butyl-3-methylimidazolium ($C_4$mim) bis(trifluoromethanesulfonyl)imide (TFSI), the addition of water yields an increase of the diffusion and the systems tends to separate the molecular species much before the demixing concentration (Rollet et al., 2007); on the contrary, the addition of lithium cation induces a great decrease of the diffusion (Jayakody et al., 2020; Monteiro et al., 2008; Ngo et al., 2022), that is due to the strong interaction of lithium with the TFSI anion (Lassègues et al., 2009; Monteiro et al., 2008). In this paper, we have focused on this question from the dynamical point of view, and in the case where the supplementary species are monoatomic cations. We have chosen one monovalent cation $Li^+$ and one multivalent cation $La^{3+}$.

The importance of the couples IL/$Li^+$ and IL/$La^{3+}$ emerges in advanced technologies. The couple IL/$Li^+$ is the subject of numerous studies related to lithium batteries and supercapitors (Lewandowski and Świderska Mocek, 2009). In these kinds of applications, transport aspects are obviously critical, and more specifically, the one of lithium

* Corresponding author.
*E-mail addresses:* anne-laure.rollet@sorbonne-universite.fr (A.-L. Rollet), guillaume.meriguet@sorbonne-universite.fr (G. Mériguet).

https://doi.org/10.1016/j.jil.2024.100087
Received 16 November 2023; Received in revised form 12 March 2024; Accepted 12 March 2024
Available online 19 March 2024

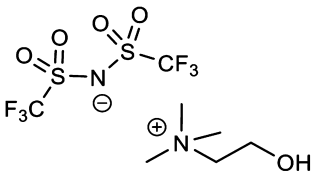

**Fig. 1.** Chemical structure of [Chol][TFSI].

transport. The decrease of the diffusion of the different species upon increasing the lithium concentration is a major problem, even a blocking point (Lewandowski and Świderska Mocek, 2009).

The couple IL/$La^{3+}$ is encountered in the waste recycling domain. Several studies propose the use of ionic liquids for the liquid-liquid extraction step in the hydrometallurgy processes (Dai et al., 1999; Okamura and Hirayama, 2021). Indeed, ionic liquids can be used both as solvent and as extractant for critical metal, like rare earth elements (REE), in liquid-liquid extraction. In this kind of processes, the extraction and separation efficiency of REE is often significantly enhanced in comparison with those using common organic solvents (Dai et al., 1999; Okamura and Hirayama, 2021). In this case also, the transport of the different species is crucial. Surprisingly, there are very few studies on mixtures of ionic liquids and other monoatomic cation than lithium. The studies dealing with other cation mostly concern other monovalent cation, in the aim of evaluating their interest for battery (Ngo et al., 2022; Taige et al., 2012; Vicent-Luna et al., 2018).

In this context, we follow a broad approach of the question by studying the dynamic of the different species over a wide window of observation time, spanning from the nanosecond to the second approximately. To cover this range of nine orders of magnitude, we have combined pulsed field gradient (PFG) nuclear magnetic resonance (NMR) technique to the NMR relaxometry performed at various fields, from 0.0002 T to 11.7 T (i.e. from 10 kHz to 500 MHz at $^1$H frequency). Specifically, fast field cycling (FFC) relaxometry, PFG diffusion and two-dimensional methods further probe molecular motions over a range of timescales (Kimmich, 1997, 2012, 2019). The Pulsed Field Gradient (PFG) NMR technique allows the determination of the self-diffusion coefficients of molecules and ions at the micron scale, by labeling, thanks to pulsed magnetic field gradients, their spins according to their spatial position (Callaghan, 2014; Johnson, 1999; Price, 2009). Easy to implement and fast, it is probably the most employed method to measure self-diffusion coefficients in various media, from the common aqueous solutions (Johnson, 1999) to high temperature molten salts (Rollet et al., 2009), confined liquids (Callaghan, 2014; Rollet et al., 2001) and even solids (Fujara et al., 2008). At the micron scale, the measured diffusion coefficients contained many shorter dynamical processes. This is particularly significant in porous media, where the molecule diffuses inside pores and between pores regimes, but also interacts more or less strongly with the pores (possible intermittent adsorption) (Kimmich, 1997, 2019; Korb, 2018). To access this intermediate time scale, the only choice is to use NMR relaxometry. Although there is no pore walls in ILs considered here, their structure and dynamics are known to be complex (Berrod et al., 2017; Ferdeghini et al., 2017) and NMR relaxometry may reveal their several different characteristic time scales. At low field, NMR relaxometry can also allow us to determine the translational diffusion coefficient, hence connecting with the time scale of the PFG NMR technique (Kruk et al., 2014).

The ionic liquid chosen for this study is the cholinium bis(trifluoromethanesulfonyl)imide [Chol][TFSI]. The particularity of this IL is that it carries a hydroxyl group on its alkyl chain (Fig. 1). This hydroxyl group induces some clustering of the cation via its hydroxyl tail. How is the hydroxyl group involved in the solvation of lithium and lanthanum ions? Does the hydroxyl group improve or impede solvation and transport? The current study addresses these questions by investigating dynamics using NMR techniques.

## 2. Experimental

### 2.1. Synthesis of the ionic liquid

Cholinium bis(trifluoromethanesulfonyl)imide, [Chol][TFSI], was prepared following a literature procedure (Nockemann et al., 2009) using Lithium bis(trifluoromethanesulfonyl)imide, Li(TFSI) (> 99%, Solvionic), and N-(2-hydroxyethyl)-N,N,N-trimethylammonium (cholinium) chloride (≥ 98.0%, Sigma-Aldrich). Li(TFSI) (0.43 mol, 123.55 g) dissolved in water (25 mL) was added to a solution of cholinium chloride (0.43 mol, 60.08 g) in water (25 mL). The mixture was vigorously stirred one hour at room temperature after which, two phases were observed. The IL phase was separated. To remove chloride impurities, IL phase was washed with water until the addition of silver ions did not yield an AgCl precipitate. The [Chol][TFSI] IL was freeze-dried and was obtained with an average yield of 74%. The molecular structure of [Chol][TFSI] is shown in Fig. 1. $^1$H NMR (300 MHz, DMSO-d6, $\delta$ ppm): 5.27 (t, 1H), 3.84 (m, 2H), 3.39 (m,2H), 3.10 (s, 9H).

### 2.2. Sample preparation

Lithium bis(trifluoromethanesulfonyl)imide, Li(TFSI) (> 99%, Solvionic), and Lanthanum(III) bis(trifluoro-methanesulfonyl)imide, $La(TFSI)_3$ (> 99.5%, Solvionic) were used to prepare salt solution in the ionic liquid.

After [Chol][TFSI] was freeze dried, the ionic liquid and the salts Li(TFSI) and $La(TFSI)_3$ were further dried in a vacuum furnace at 80 °C before being inserted in a glove box under argon atmosphere, to avoid water intake in the sample. $Li^+$ and $La^{3+}$ solutions in [Chol][TFSI] are obtained by adding increasing mass of Li(TFSI) or $La(TFSI)_3$ in the ionic liquid [Chol][TFSI] in the inert atmosphere of a glove box. Li(TFSI) was mixed by using a sonicator and the mixture was heated at 40 °C (above the [Chol][TFSI] melting of 27 °C) until a clear liquid was formed, $La(TFSI)_3$ was added to [Chol][TFSI] and the mixture was heated to 125 °C during 30 min. The solutions were introduced into the NMR tubes and then flame-sealed under vacuum using a tip-off manifold (Wilmad-Labglass) before use.

The obtained $Li^+$ solutions were liquid at room temperature for Li molality between 0.05 mol $kg^{-1}$ and 2.5 mol $kg^{-1}$ and solid otherwise. Hereafter the compositions will be referred to as mole fraction of salts defined as:

$$x_{\mathrm{LiTFSI}} = \frac{n_{\mathrm{LiTFSI}}}{n_{\mathrm{LiTFSI}} + n_{\mathrm{CholTFSI}}} \qquad x_{\mathrm{La(TFSI)_3}} = \frac{n_{\mathrm{La(TFSI)_3}}}{n_{\mathrm{La(TFSI)_3}} + n_{\mathrm{CholTFSI}}} \quad (1)$$

### 2.3. NMR

All experiments were carried out at 40 °C, where all the $Li^+$ and $La^{3+}$ solutions were liquid.

*NMR spectroscopy* $^1$H-$^{19}$F and $^{19}$F-$^7$Li HOESY experiments were performed using the 5 mm Jeol JNM-ECZ, Royal HFX probe, at a magnetic field of 9.4 T ($^1$H Larmor frequency of 400 MHz) and processed with the JEOL Delta software. Operating this probe at dual tune mode allows us to perform a series of advanced experiments, which includes $^{19}$F-$^7$Li HOESY. $^1$H-$^7$Li 2D heteronuclear NOE were carried out with a 500 MHz (11.7 T) Bruker AV III spectrometer equipped with 5 mm Double Resonance Broadband Probe (BBI). The mixing time was varied from 0.1 to 2 seconds for each sample to find the optimal time.

*PFG NMR* NMR Pulsed Field Gradient (PFG) measurements were performed on a 300 MHz and a 500 MHz Bruker spectrometers at 40 °C. The first one was equipped with a probe capable of producing magnetic field gradient pulses up to of 50 G $cm^{-1}$ for $^1$H and 120 G $cm^{-1}$ for $^7$Li and $^{19}$F experiments. The second one was equipped with a probe of maximum strength gradient of 55 G $cm^{-1}$ for $^1$H experiments. The diffusion measurement was conducted with a 2D sequence using stimulated

echo and longitudinal eddy current delay with bipolar gradients (Wu et al., 1995). The gradient pulse duration $\delta$ and the diffusion time $\Delta$ were in the range of 1 to 10 ms and 0.2 to 2 s, respectively. The gradient strength $g$ was varied from 2 to 98% of the maximum strength in 16 steps. The diffusion coefficients $D$ were determined by fitting the echo signal decay with the equation (Wu et al., 1995):

$$I(g) = I(0)\mathrm{e}^{-Dq^2\left(\Delta-\frac{\delta}{2}-\frac{\tau}{2}\right)} \tag{2}$$

where $q = \gamma G\delta$ and $\tau$ is a delay between bipolar gradient pulses.

*High field relaxation* The longitudinal relaxation rates for $^1$H, $^7$Li were measured at 300 MHz and a 500 MHz, and only at 300 MHz for $^{19}$F, using the same spectrometers as for PFG NMR experiments. Inversion-recovery pulse sequence was used, with 16 relaxation delays optimized for each $T_1$ value, typically varying from 500 µs to 5 s.

*Fast Field Cycling (FFC) NMR* The $^1$H NMR relaxation rate dispersion was measured with a Fast Field Cycling NMR relaxometer Spinmaster Duo (Stelar s.r.l., Italy). The relaxation field were varied from 10 kHz to 40 MHz. For frequencies below 12 MHz, the pre-polarized (PP) sequence was used with a polarization field of 20 MHz whereas the non-polarized (NP) was applied for higher frequencies (Anoardo et al., 2001). The detection field was 16.29 MHz and the duration of the 90° pulse set to 9 µs. The recycle delay (time between the repetition of each sequence) was set to 5 times the longest $T_1$. The field switching time between the different magnetic fields was chosen to be 3 ms. Magnetization values were recorded for 32 logarithmically spaced values of relaxation delays in the approximate range $0.01T_1 - 4T_1$. In the whole frequency range explored, the relaxation curves were satisfactorily fitted with monoexponential function within experimental error. The temperature was kept at $40 \pm 1$ °C thanks to a gas flow regulated by a VTC 91 temperature controller (Stelar s.r.l., Italy).

## 3. Spin relaxation theory

The longitudinal relaxation time $T_1$ (rate $R_1$) is the characteristic time of the return to equilibrium of the component of magnetization along $B_0$ magnetic field after a perturbation (Abragam, 1961). This relaxation originates from the temporal fluctuations of the magnetic field, i.e. the fluctuations of the $^1$H-$^1$H or $^{19}$F-$^1$H dipole-dipole in the ionic liquid under study.

Both intramolecular or intermolecular interactions can be at the origin of the relaxation process, and when they can be decoupled, the observed relaxation rate $R_1$ is the addition of all the contributions. For $^1$H, the measured relaxation rate $R_1(\omega)$ can be described as below

$$R_1 = R_{1,\mathrm{intra}} + R^{HH}_{1,\mathrm{inter}} + R^{HF}_{1,\mathrm{inter}} \tag{3}$$

where $R_{1,\mathrm{intra}}$ is the internal cation contribution ($^1$H-$^1$H), $R^{HH}_{1,\mathrm{inter}}$ the cation-cation contribution ($^1$H-$^1$H) and $R^{HF}_{1,\mathrm{inter}}$ the anion-cation contribution ($^{19}$F-$^1$H). $R_{1,\mathrm{intra}}$ can be complex due to the number of internal motions to considered, but often this contribution is reduced to the overall tumbling of the cation and is expressed as:

$$R_{1,\mathrm{intra}}(\omega) = C_{DD}\left[J_{\mathrm{intra}}(\omega) + 4\,J_{\mathrm{intra}}(2\omega)\right] \tag{4}$$

$C_{DD}$ is a constant depending on spin factors and geometry and $J_{\mathrm{intra}}(\omega)$ is the spectral density (Fourier transform of the autocorrelation function) corresponding to the tumbling motion. The simplest way to model it, is to describe it as a continuous rotational diffusion with a rotational correlation time $\tau_\mathrm{r}$. In this case, $J_{\mathrm{intra}}(\omega)$ is a Lorentzian function, that has already been successfully used to fit NMRD profiles of ionic liquids (Bloembergen et al., 1948; Honegger et al., 2020; Jayakody et al., 2020; Kruk et al., 2016, 2020; Ordikhani-Seyedlar et al., 2015; Overbeck et al., 2020).

$$J_{\mathrm{intra}}(\omega) = \frac{\tau_\mathrm{r}}{1 + \left(\omega\tau_\mathrm{r}\right)^2} \tag{5}$$

In some liquids, the tumbling cannot be described by a single correlation time and a distribution of correlations times has to be employed. To take this observation into account, a more elaborated Cole-Davidson model (inspired from dielectric spectroscopy) can be used (Beckmann et al., 2022; Kruk et al., 2012, 2014; Overbeck et al., 2021; Wencka et al., 2017) and leads to the following expression of the spectral density.

$$J_{\mathrm{intra}}(\omega) = \frac{\sin\left[\beta \arctan(\omega\tau)\right]}{\omega\left[1 + (\omega\tau)^2\right]^{\frac{\beta}{2}}} \tag{6}$$

with $\tau_\mathrm{r} = \beta\tau$. $\beta$ is a stretching parameter with $0 < \beta \leq 1$. For $\beta = 1$, the Lorentzian form of eq. (5) is recovered.

$R^{HH}_{1,\mathrm{inter}}$ and $R^{HF}_{1,\mathrm{inter}}$ contributions are caused respectively by the cation-cation and anion-cation distance fluctuations (Fraenza and Greenbaum, 2022; Kruk et al., 2014; Overbeck et al., 2020). The simplest model is to consider that anion and cation are diffusing independently and only limited by a distance of closest approach (Ayant et al., 1975; Hwang and Freed, 1975). This model is often referred to as the force free hard-sphere (FFHS) model of translational diffusion and leads to the following expressions.

$$R^{HH}_{1,\mathrm{inter}}(\omega) = \frac{8}{5}\frac{\pi\hbar^2\gamma_H^4 N_H I(I+1)}{bD_{HH}}\left[J_{\mathrm{inter}}(\omega) + 4\,J_{\mathrm{inter}}(2\omega)\right] \tag{7}$$

$$R^{HF}_{1,\mathrm{inter}}(\omega) = \frac{8}{15}\frac{\pi\hbar^2\gamma_H^2\gamma_F^2 N_F I(I+1)}{bD_{HF}}\left[J_{\mathrm{inter}}(\omega-\omega_F) + 3\,J_{\mathrm{inter}}(\omega) + 6\,J_{\mathrm{inter}}(\omega+\omega_F)\right] \tag{8}$$

with the corresponding spectral density (Ayant et al., 1975; Kowalewski and Mäler, 2006)

$$J_{\mathrm{inter}}(\omega) = \frac{\frac{3}{2}u^2 + \frac{15}{2}u + 12}{\frac{1}{8}u^6 + u^5 + 4\,u^4 + \frac{27}{2}u^3 + \frac{81}{2}u^2 + 81\,u + 81} \tag{9}$$

$u = \sqrt{2\omega\tau_D}$, $\tau_D$ is the translational correlation time which is computed as $\tau_D = \frac{b^2}{D_{ij}}$, $b$ denotes the distance of closest approach between the $^1$H spin and another cation or an anion, $D_{ij} = D_i + D_j$ is the relative translational diffusion coefficient given as the sum of diffusion coefficients of the interacting species $i$ and $j$. The quantities $N_H$ and $N_F$ denote the number of $^1$H and $^{19}$F nuclei per unit volume.

During the fitting process of the relaxation dispersion curves, due to the large number of adjustable parameters, some of them were constrained. $N_H$ and $N_F$ were fixed to the values computed from the density of the ionic liquid. The best distance of closest approach was found to be $b = 5$ Å. The diffusion coefficient of the anion $D_{\mathrm{TFSI^-}}$ was fixed to the value determined by $^{19}$F PFG-NMR while the diffusion coefficient of the cation $D_{\mathrm{Chol^+}}$ was set free for comparison to the value determined by $^1$H PFG-NMR. $\tau$ and $\beta$ were free parameters.

For ionic liquids, this description was questioned by Driver et al. (2017) with a combination of Fast Field Cycling relaxometry and Molecular dynamics. They suggested that for [$C_4$mim][$PF_6$], the low-frequency contribution rather stems from long time correlated reorientational modulations than translational diffusion. However, Honegger et al. (2020) using the same techniques on [$C_2$mim][$N(CN)_2$]) showed that the low-frequency contribution is caused by translational diffusion.

## 4. Results and discussion

### 4.1. Diffusion at long scale

The diffusion at the micrometer scale was investigated for [Chol][TFSI] + LiTFSI on one hand and for [Chol][TFSI] + La[TFSI]$_3$ on the other hand. Self-diffusion coefficients of $Chol^+$, $Li^+$ and $TFSI^-$ were measured independently by considering the signals of the $-N-CH_2$

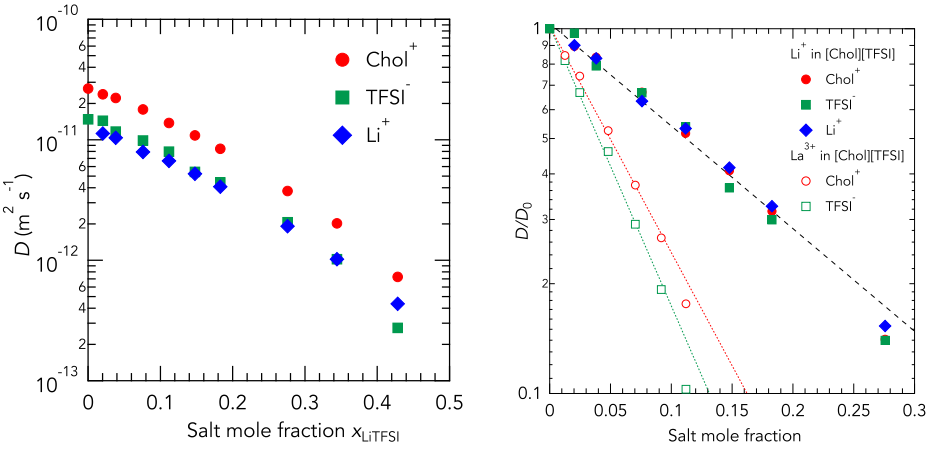


**Fig. 2.** *Left:* Self-diffusion coefficient of $Chol^+$, $TFSI^-$ and $Li^+$ vs the mole fraction of Li(TFSI), $x_{LiTFSI}$. *Right:* Reduced diffusion coefficients vs the salt mole fraction for lithium and lanthanum solutions. Dotted and dashed lines are guides for the eye.

group, $-CH_2-O$ group and methyl group ($-CH_3$) on the $^1H$ NMR spectrum of cholinium, $CF_3$ group on the $^{19}F$ NMR spectrum of bis(trifluoromethanesulfonyl)imide, and simply the single peak on the $^7Li$ lithium of spectrum.

We present first the results for the [Chol][TFSI] + LiTFSI mixtures and after will compare them to those for [Chol][TFSI] + La[TFSI]$_3$. The self-diffusion coefficients of cholinium ($^1H$), TFSI ($^{19}F$) and lithium ($^7Li$) ions decrease of LiTFSI (Fig. 2) about two orders of magnitude from the infinite dilution to 3 mol/kg, i.e. $x_{Li(TFSI)} = 0.5$. Such decrease when adding lithium salt in ionic liquids has been observed, along with an increase of the viscosity, for all the studied systems: imidazolium type with LiTFSI (Lesch et al., 2014; Monteiro et al., 2008, 2010; Ngo et al., 2022; Saito et al., 2007; Srour et al., 2015; Tsuzuki et al., 2010), $LiBF_4$ (Haskins et al., 2014; Hayamizu et al., 2004; Judeinstein et al., 2021; Wu et al., 2012) or $LiPF_6$ (Saito et al., 2007), pyrrolidinium kind with LiTFSI (Borodin et al., 2006; Haskins et al., 2014; Li et al., 2012; Nicotera et al., 2005; Solano et al., 2013) or $LiPF_6$, ammonium kind (Hayamizu et al., 2008; Le et al., 2010), and other less common ionic liquids (Monteiro et al., 2010). The density of the liquid also often increases upon lithium salt addition.

Nevertheless, the decrease depends on the ionic liquids. In the case of [Chol][TFSI], it is by far the strongest observed, as it is usually less than one order of magnitude. The slowdown of the dynamics in ionic liquids containing lithium cations has been related to a modification of the structure of the liquid, through the solvation of lithium (Aguilera et al., 2015; Lassègues et al., 2006; Li et al., 2012; Monteiro et al., 2008) and even with possible clustering of lithium (Haskins et al., 2014; Lesch et al., 2014). In the case of TFSI anion, lithium cation interacts more strongly with the oxygen (Xu et al., 2022; Yang et al., 2022) and is surrounded by approximately three TFSI. Experimentally, the solvation of lithium cation by TFSI anion, is expressed by the evolution of $D_{TFSI}$ that tends to come closer to $D_{Li}$ when $Li^+$ concentration is increased. In this regard, the effect of anion on transport in lithium/ionic liquids system has been more often investigated. The very symmetric $BF_4^-$ anion yields a very slow diffusion of $Li^+$, despite $D_{BF_4}$ remains close to the diffusion value of the ionic liquid cation (Hayamizu et al., 2004; Judeinstein et al., 2021; Wu et al., 2012), whereas for TFSI, the diffusion of lithium remains close to other ionic species (Monteiro et al., 2008, 2010; Ngo et al., 2022; Saito et al., 2007; Tsuzuki et al., 2010). From this comparison emerges the picture of a strong solvation of lithium by $BF_4^-$ and a loose solvation by TFSI anion, in agreement with the binding energy calculated by Molecular Dynamics Simulations (Haskins et al., 2014). It can be also underlined that $BF_4^-$ is centrosymmetric whereas TFSI anion is not, and one can suspect that it has an impact on the modification lithium solvation with its concentration. This idea of asymmetry has been pushed forward by mixing asymmetric anions (Xu et al., 2022) leading to better transport performance for lithium.

Another interesting observation in Fig. 2, is the crossing of $D_{Li}$ and $D_{TFSI}$ around $x_{Li(TFSI)} = 0.35$, below this mole fraction $D_{TFSI} > D_{Li}$ and above $D_{Li} > D_{TFSI}$. Note that in pure molten lithium bis(fluorosulfonyl)imide and lithium fluorosulfonyl(trifluoromethylsulfonyl)imide $D_{Li} > D_{anion}$ with the respective values of $D_{Li} = 1.4 \times 10^{-11}$ m$^2$/s, $D_{FSI} = 5.5 \times 10^{-12}$ m$^2$/s and $D_{Li} = 7 \times 10^{-12}$ m$^2$/s, $D_{FTSI} = 0.7 \times 10^{-12}$ m$^2$/s (Measurements performed at 423 K) (Kubota et al., 2018).

Again, the structure of the different [Chol][TFSI]+LiTFSI mixtures can be questioned. Many studies, using either scattering techniques, or spectroscopy, or simulations, have been devoted to the structure of the liquid when lithium cations are present. Despite the lack of full agreement, a picture of the system can be drawn. In the different ILs/lithium mixtures studied in the literature, lithium cation is coordinated by the oxygen of the TFSI and rarely by the nitrogen (Castriota et al., 2005; Lassègues et al., 2006; Li et al., 2012; Monteiro et al., 2008; Solano et al., 2013; Umebayashi et al., 2011; Xu et al., 2022). When considering the radial distribution function (RDF), they clearly show the following order in the proximity to lithium: oxygen, nitrogen, fluorine. This intermediate distance between lithium and fluorine atoms is confirmed by our $^{19}F$-$^7Li$ HOESY experiment (Fig. S7 of the SI)). TFSI solvates $Li^+$ by the coordination of either one (monodentate) or two (bidentate) of its four oxygen atoms. Studies using Raman spectroscopy combined with ab initio calculations show that TFSI cis isomer solvates preferentially the lithium in comparison with the trans isomer, and bidentate configuration is the most common (Lassègues et al., 2006; Umebayashi et al., 2010). Furthermore, they strongly suggest that $Li^+$ is solvated by four oxygens and two TFSI anions. The number is a matter of debate, as numerical simulations find that the mean coordination number of lithium by TFSI about 3, for the different kinds of ILs studied (imidazolium, pyrrodylinium and ammonium) and does not change much with the lithium concentration (Haskins et al., 2014; Li et al., 2012; Monteiro et al., 2008; Solano et al., 2013; Xu et al., 2022). As pointed out by Umebayashi et al. (2011) in their study, the radial distribution function of nitrogen consists in two close peaks at 3.6 and 4.3 Å attributed to bidendate and monodentate conformation, respectively. Hence, the issue is to define where is the first solvation shell. At high concentration, the lithium affects strongly the long distance organization of the liquid (Umebayashi et al., 2011).

More interestingly, the local organization around $Li^+$ ions changes with lithium concentration. Again, the publications disagree on this point. Numerous structural studies based on Raman spectroscopy indicate a decrease of the coordination number along with keeping the cis isomer conformation and bidentate configuration (option 1), while most of numerical simulations indicate that at low concentration, $Li^+$ is

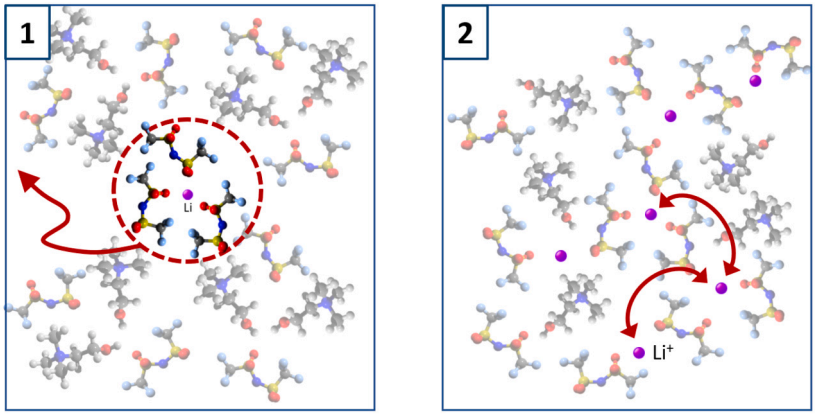


**Fig. 3.** Scheme of two different transport mechanisms of $Li^+$ in [Chol][TFSI]: 1) vehicular mechanism: $Li^+$ moves with its solvation shell; 2) hopping mechanism: $Li^+$ jumping from one TFSI solvation cage to another.

solvated by both monodentate and bidentate TFSI, but as $Li^+$ concentration increases, the monodentate coordination along with a sharing of TFSI between two lithium becomes predominant (option 2) (Li et al., 2012; Tong et al., 2020; Umebayashi et al., 2011; Xu et al., 2022). What can we learn from the study of dynamics?

In option 1, the lithium transport may probably be of vehicular kind, i.e. lithium moves with its solvation sphere, whatever the concentration. In option 2, the modification of the structure operates a change between a vehicle transport mechanism, to a hopping mechanism, i.e. lithium jumping from one TFSI solvation cage to another. These two transport mechanisms are illustrated in Fig. 3.

The crossover between $D_{TFSI}$ and $D_{Li}$ observed in Fig. 2 can be interpreted as an experimental evidence of a change in the mechanism transport of lithium, the later passing from vehicle kind at low lithium concentration to hopping kind at high concentration. Similar interpretation has been performed by Dokko et al. (2018), who have evidenced using PFG NMR such change in the lithium transport mechanism for sulfolane + $LiBF_4$ mixtures. The change occurs around $x_{Li(TFSI)} = 0.35$ in [Chol][TFSI] that would correspond, if one considered that it was the mole fraction for which all the TFSI anions were involved in the solvation of lithium, to a coordination number of about 2.9. It can be noticed that a change between vehicular and Grotthuss transport mechanisms has been evidenced proton ionic liquids (Anouti et al., 2010).

The effect of the ionic liquid cation cannot be ruled out. In general, the diffusion slowdown upon lithium salt addition, is greater in the imidazolium family than in the ammonium one, except for the cholinium. The hydroxyl group has a great impact on the liquid structure because the H-bond makes it possible the existence of clusters of cation, here cholinium (Khudozhitkov et al., 2023; Niemann et al., 2019; Strate et al., 2017). In the case of [Chol][TFSI], Nockemann et al. (2009) have shown that in its crystal structure, the hydroxyl group was pointing to the oxygen of the TFSI anion, making H-bond. We have seen that lithium is solvated by the oxygen of the TFSI anion instead of the nitrogen, despite the later is more negatively charged (Tsuzuki et al., 2010), strongly suggests that the hydroxyl group of the cholinium can participate to the lithium solvation. In order to probe the proximity of lithium and the hydroxyl group, $^7$Li-$^1$H HOESY experiment has been carried out (Fig. 4) at different mole fractions. Thanks to the Overhauser effect, the spatial proximity, within 5 Å approximately, of two nuclei of the same nature (NOESY) and different nature (HOESY) can be evidenced. In Fig. 4, a cross peak is clearly visible between lithium and the hydrogen of the hydroxyl group for $x_{LiTFSI} = 0.02$. The organic cation may thus impact the coordination (monodentate/bidentate) of the lithium. Counter-intuitively, at high $x_{LiTFSI}$, there is no more cross peak, meaning cholinium cation is expelled from the solvation shell of lithium, by increasing the amount of the latter.

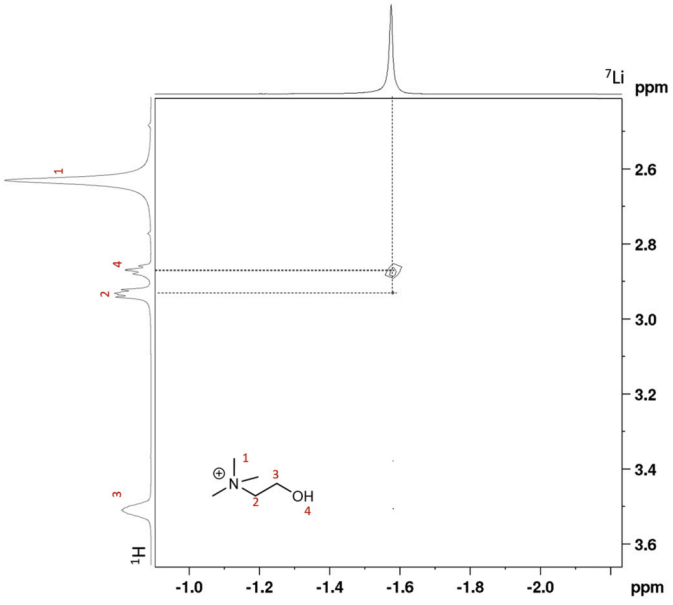


**Fig. 4.** $^1$H-$^7$Li HOESY of [Chol][TFSI] with $x_{LiTFSI} = 0.02$, recorded at 11.7 T.

This strong modification of the OH environment is also visible in the NMR spectra (Fig. S1 of the SI). The peak of the OH shifts toward high chemical shift values, i.e. there is a deshielding of the $^1$H, upon lithium addition. The comparison with the $^1$H chemical shifts in the following three systems, neat [Chol][TFSI] (+2.84 ppm), [Chol][TFSI] diluted in d6-DMSO (+5.23 ppm) (Fig. S2 of the SI) and LiOH (−1.5 ppm) (Liu et al., 2017), suggests that the addition of lithium in [Chol][TFSI] leads to the disappearance of the H-Bond between the hydroxyl groups.

The dynamics of the [Chol][TFSI] has also been investigated upon the addition of $La(TFSI)_3$. The reduced self-diffusion coefficients $D/D_0$, where $D_0$ is the self-diffusion coefficient for neat [Chol][TFSI], are presented in Fig. 2 and compared with those of the mixtures with LiTFSI. The decrease of both cholinium and TFSI $D/D_0$ upon salt addition is notably stronger with $La^{3+}$ than those with $Li^+$. This is consistent with the stronger increase of viscosity upon adding multivalent cation than adding monovalent cation (Ngo et al., 2022; Vicent-Luna et al., 2018). As expected, the TFSI diffusion is more affected than cholinium one (note that it was not possible to measure the self-diffusion coefficient of lanthanum by PFG NMR). These results are in line with the scarce studies considering the diffusion in ionic liquids containing multi-valent ions. The simulations of Vicent-Luna et al. (2018) on a large series of mixtures of 1-butyl-1-methyl-pyrrolidinium TFSI and $M(TFSI)_n$ showed that the more charged ion, the stronger the decrease of the diffusion. It

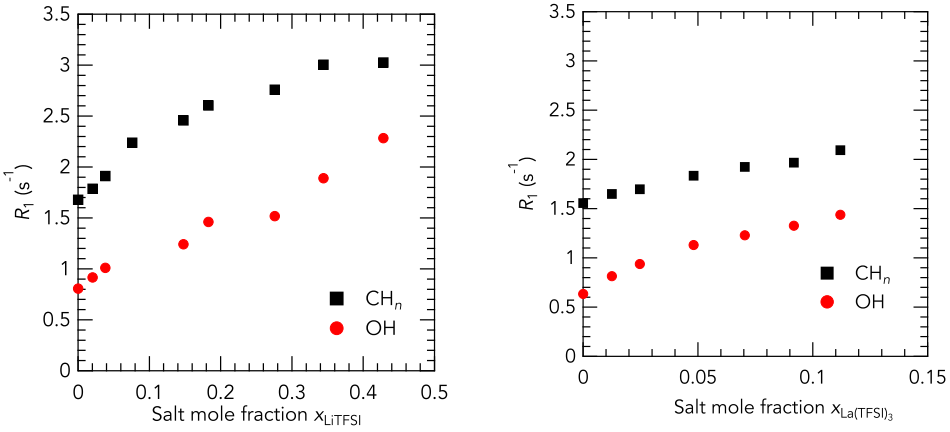


**Fig. 5.** Evolution of the $^1$H longitudinal relaxation rate $R_1$ at 300 MHz, vs the mole fraction of $Li^+$ (left) and vs the mole fraction of $La^{3+}$ (right).

is correlated to the solvation of the inorganic cation by the oxygen of the TFSI anion. The more charged, the higher the coordination number Vicent-Luna et al. (2018).

### 4.2. NMR relaxation at high field

To have a better insight into the phenomenon at play, this long distance transport study (PFG NMR investigates micrometer scale diffusion), needs to be completed by study at a more local scale.

To understand how the inorganic cations impact the dynamics of the ionic liquids at short timescale, the NMR relaxation rates $R_1$ of $^{19}$F and $^1$H of all chemical groups was then measured. Indeed, $R_1$ gives insight into to the dynamics at timescale around $1/\omega_0$, i.e. in the present case at the nanosecond timescale (Korb, 2018). Hence it gives insight into how local motions affect long range motions. For $^1$H carried by the cholinium, there are two groups of relaxation rates: one related to the $CH_n$ groups ($R_1$ about 1.5 s$^{-1}$ in neat IL) and one related to the OH group ($R_1$ about 0.7 s$^{-1}$). All the values are gathered in the supplementary information file. Then, for the sake of readability, the relaxation rates of the protons of the groups $-CH_3$, $-CH_2-N$ and $-CH_2-O$ of the $Chol^+$ cation were averaged and reported as $CH_n$ in Fig. 5.

For both the $^1$H (all the chemical groups of cholinium) one observes an increase of $R_1$ with $x_{LiTFSI}$ or $x_{La(TFSI)_3}$. However, there are significant differences. First, the $^1$H $R_1$ of OH is much smaller than those of $CH_n$. The source of relaxation for $^1$H being dipole-dipole interaction, it appears as if, either the distances with other $^1$H or $^{19}$F are higher, or the proton dynamics of OH is much faster by exchange with other OH. One can also notice that the evolution of $R_1$ of OH seems to converge with the $R_1$ of $CH_n$ at high $x_{LiTFSI}$ and $x_{La(TFSI)_3}$. This trend is more pronounced at 500 MHz (Fig. S8 of the SI). It may indicate that the dynamics of all the choline groups become similar and correspond to rotation of the whole organic cation. Furthermore, it suggests that the H-exchange between OH disappears.

To go further $^{19}$F, as well as $^7$Li relaxation rates have been measured and their evolution with mole fraction is plotted in Fig. 6 (it was not possible to measure $^{139}$La with our spectrometer due to the proximity of its resonance frequency to the one of $^2$H used for the $B_0$ field lock). Whereas the increase for all the $^1$H is continuous all over the concentration range, for the $^{19}$F, a plateau is reached around $x_{LiTFSI} = 0.15$ for lithium and $x_{La(TFSI)_3} = 0.05$ for lanthanum. This phenomenon demonstrates a different evolution of the dynamics for the cholinium and for the TFSI, as already pointed out previously with our diffusion results.

At this point, it is interesting to look at the $^7$Li $R_1$ variation with $x_{LiTFSI}$ (Fig. 6). Here, it is important to recall that $^{19}$F has 1/2 spin and its NMR relaxation is ruled by the dipole-dipole interaction and by the chemical shift anisotropy (CSA) interaction, whereas $^7$Li has 3/2 spin and its NMR relaxation is ruled by the dipole-dipole interaction and the quadrupolar interaction. The complex aspect for $^7$Li is that none of these two interactions clearly dominates and both have to be considered. To be more precise, for the dipolar interaction it corresponds to the relative fluctuation of two magnetic dipoles, whereas for the quadrupolar interaction it corresponds to the fluctuation of the electric field gradient experienced by the nucleus (Kimmich, 1997). Despite their different relaxation mechanisms, the evolution of the relaxation rates of the two nuclei can be compared. The $^7$Li $R_1$ is constant up to $x_{LiTFSI} = 0.15$ and decreases above this amount in LiTFSI (Fig. 6). This striking concomitant change of $^{19}$F $R_1$ and $^7$Li $R_1$ shows how their respective dynamics is intertwined, but in apparent opposite direction. Furthermore, the $^7$Li chemical shift variation with $x_{LiTFSI}$ exhibits a change at the very same mole fraction (figures shown in the SI).

Hence, the plateau observed for $^{19}$F could correspond to this state of the liquid structure where each TFSI ion coordinates two lithium ions via their oxygens creating this way a labile network, similar to those evidenced in molten fluoride salts (Rollet and Salanne, 2011; Rollet et al., 2008). The TFSI anions, “trapped” in this network, have in a way a restricted dynamics. At local scale, the dominant motion of $CF_3$, from the NMR point of view, is the rotation of the molecular group.

The reverse variation of $^7$Li $R_1$, i.e. plateau followed by a decrease suggests the following scene. Up to approximately $x_{Li(TFSI)} = 0.15$, Lithium is solvated similarly by TFSI anions, i.e. it has the same coordination number. Above this concentration, TFSI anions are shared between several lithium and create a labile network. Lithium ions can then jump from site to site. These jumps increase the lithium mobility that leads to a decrease of $R_1$. Interestingly, in mixture of n-methyl-n-propylpyrrolidinium bis- (trifluoromethanesulfonyl)imide ([PYR13][TFSI]) and 1- ethyl-3-methylimidazolium dicyanamide ([EMIM][DCA]) (ratio 1:9) and LiTFSI, the picture seems different, as the lifetime of TFSI around Lithium decreases with the concentration of lithium because of the exchange with DCA anions. (Huang et al., 2019) Nevertheless, the long range diffusion of lithium continuously decreases with LiTFSI mole fraction (Fig. 2) and rules out the increase of the lithium mobility at long range, but not the jump diffusion process. A decrease of the mobility can also yield to a $R_1$ decrease, as in the famous BPP (Bloembergen-Purcell-Pound) model (Bloembergen et al., 1948). In the later, the dynamics is described by a rotational diffusion of characteristic time $\tau_r$, that is expressed in the frequency domain by a Lorentzian (equation (5)). When $\tau_r$ becomes higher than the Larmor frequency, $R_1$ decreases. In the present case, rotational diffusion does not seem suitable and $^7$Li $R_1$ dispersion profile would be important information to reveal the dynamics at the intermediate timescale.

Despite the NMR relaxation data at 300 and 500 MHz do not fully reveal the dynamics of cholinium, TFSI and lithium, they evidence the modification of the dynamics of TFSI and lithium due to the change of solvation of lithium by TFSI. The labile network that progressively leads to an inversion of the self-diffusion coefficients of TFSI and lithium

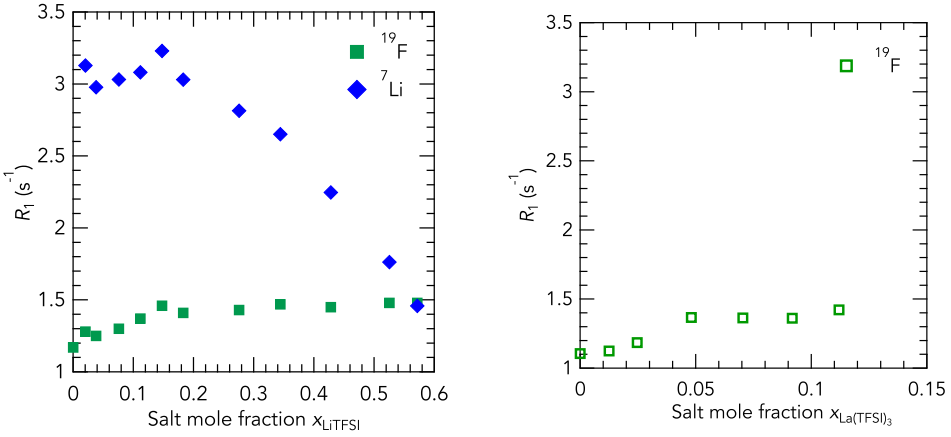


**Fig. 6.** Evolution of the $^{7}$Li and $^{19}$F longitudinal relaxation rates $R_1$ vs salt mole fractions LiTFSI (left) and La(TFSI)$_3$ (right) at 300 MHz ($^{1}$H).

around $x_{LiTFSI} = 0.35$, is already built at lower concentration, around $x_{LiTFSI} = 0.15$. The fact that a similar plateau (Fig. 6) is witnessed in the lanthanum systems, suggests that a change in the lanthanum transport may also occur. It can be noticed that the value of La(TFSI)$_3$ for which the plateau is reached, is a factor 3 lower than the one for lithium systems. This factor, that also separates the charge of $Li^+$ and $La^{3+}$, again points the image of the formation of a labile network within which the monoatomic cation moves by jump between one TFSI solvation cage to another. In this regard, NMR relaxation measurement brings crucial information to describe the structure and the dynamics of the mixture LiTFSI with [Chol][TFSI].

### 4.3. NMR relaxation dispersion

NMR dispersion profiles provide a wider view of the dynamics as the field is varied - consequently the time - over 4 orders of magnitude, but the price to pay is the loss of the spectral resolution. Nevertheless, as discussed in § 4.2, the relaxation rates of the protons of the groups $-CH_3$, $-CH_2-N$ and $-CH_2-O$ of the $Chol^+$ cation were found to be very close with a maximum difference of the order of 10%. The $-OH$ proton relaxation is significantly different but it represents only about 7% of the magnetization and cannot be isolated in the magnetization curves, that were satisfactorily fitted with monoexponential functions. The $^{1}$H NMR dispersion profiles are presented in Fig. 7 for lithium and in Fig. 8 for lanthanum. The introduction of ions in the ionic liquid causes an overall increase of longitudinal relaxation rate $R_1$ of the $Chol^+$ cation in the whole frequency range. This increase is more pronounced at low frequency where large scale phenomena, as translational diffusion, are causing the relaxation. The effect of the trivalent $La^{3+}$ is stronger than the one of the monovalent $Li^+$, at the same concentration. This observation is consistent with the diffusion coefficients evolution determined by PFG NMR (cf Fig. 2). In the case of TFSI, the situation is slightly different. The $^{19}$F relaxation rate increases significantly with lithium concentration at low frequency, but merges and even crosses at intermediate frequency.

To have more insight, the $^{1}$H $R_1$ dispersions were fitted according to the method detailed in section 3 and that has been successfully used for many ionic liquids. Nevertheless, the fitting failed for some of our samples. More precisely, it was possible to fit all the $^{1}$H NMRD profiles of lanthanum samples (Fig. 8) and the $^{1}$H NMRD profiles for the lithium samples up to $x_{LiTFSI} = 0.34$, but not above (Fig. 7). The fitting parameters are gathered in SI in Table S3 and S4. If the liquid became a labile network, with a change between a vehicle transport mechanism to a hopping transport mechanism for the lithium, the dynamics of the organic cation cannot be modeled by a rotational-diffusion anymore, and a more complex model has to be developed.

Below this value $x_{LiTFSI} = 0.34$, the value of the diffusion coefficient of the cation $D_{Chol^+}$ was found to be in fair agreement with the one derived from $^{1}$H PFG-NMR. $\beta$ values for all the samples were close to 1 for all the solutions investigated in the present study. From these fits, it has been possible to extract the molecular rotational characteristic time ($\tau_r$). The evolution of $\tau_r$ as a function inorganic salt mole fraction is plotted in Fig. 9. As expected, $\tau_r$ increases with $x_{LiTFSI}$ and $x_{La(TFSI)_3}$, with $\tau_r$ higher for $La^{3+}$ than for $Li^+$ at the same $x_{M(TFSI)_n}$, similarly to the order found for the long-range translational diffusion (stronger decrease of $D$ with lanthanum than with lithium). However, one can notice some differences with diffusion. On one hand, up to $x = 0.35$, these $\tau_r$ increases are smaller than translational diffusion decrease, and on the other hand, they vary differently with the salt mole fraction.

The $^{19}$F NMRD profiles for ionic liquids are scarcely measured and fitted in the literature, despite they are as easily measured as $^{1}$H NMRD profiles. The evolution of the $^{19}$F NMRD profiles with $x_{LiTFSI}$ is different of the one of $^{1}$H NMRD profiles. Whereas for $^{1}$H $R_1$ increases at all frequencies, $^{19}$F $R_1$ strongly increases only at low frequency. The $^{19}$F NMRD profiles even collapse to a common $\omega_0^{-1}$ slope in the 1-100 MHz range. The shape of the $^{19}$F NMRD profiles somehow resembles to the one of glass-forming systems (Becher et al., 2022; Carignani et al., 2018; Kruk et al., 2012). Furthermore, the model detailed in section 3 fails to reproduce the experimental curves (Fig. 7). In fact, $^{19}$F relaxation is both governed by dipolar (DD) and chemical shift anisotropy (CSA) (Gerig, 1989; Gerig et al., 1979). The difficulty is that CSA scales as $\omega_0^2$, which makes the relationship between relaxing rate and spectral density more complex. The present collected data dot not allow us to determine the proportion of DD and CSA in the relaxation rate of $^{19}$F. Nevertheless, the very strong increase $^{19}$F $R_1$ at low frequency shows that the long range dynamics is highly slowed down in accordance with the translational diffusion coefficients. The same observation was done by Jayakody et al. (2020) in the system [$C_4$mim][TFSI] + LiTFSI, nevertheless the ratio $^{19F}R_1/^{1H}R_1$ at low field is greater in their system than in [Chol][TFSI].

## 5. Conclusions

The multiscale dynamics of all the ionic species contained in mixtures of ionic liquids ([Chol][TFSI]) and inorganic salts (LiTFSI and La(TFSI)$_3$) have been studied, for concentration ranging from high dilution to saturation. The dynamical data were collected using several NMR spectrometers and relaxometers in order to get a wide times scale window (ns-s). Similarly to all the mixtures of inorganic salt and ionic liquids studied up to now, the addition of lithium and lanthanum cations yields to an important decrease of the translational diffusion of all the ionic species. The molecular rotation is also slowed down, but with a different dependence on $x_{M(TFSI)_n}$. Here, we have experimentally evidenced a change in the transport mechanism of lithium from a vehicular kind at low $x_{LiTFSI}$ to a hopping kind at high $x_{LiTFSI}$. We suspect

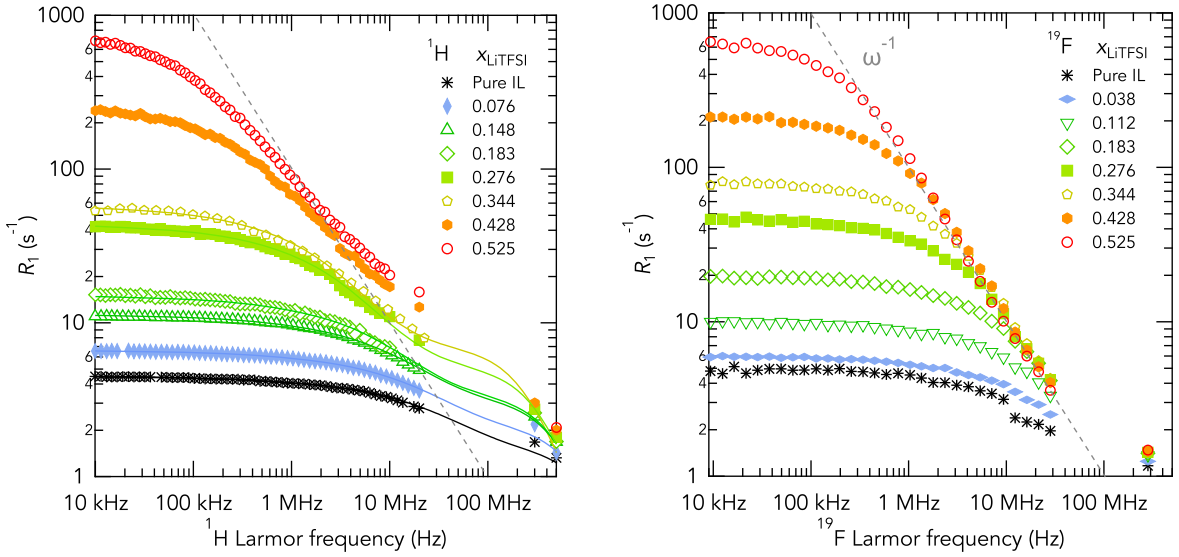


**Fig. 7.** Dispersion of the $^1$H (left) and $^{19}$F (right) longitudinal relaxation rate $R_1$ vs Larmor frequency of $Li^+$ ion solutions in [Chol][TFSI].

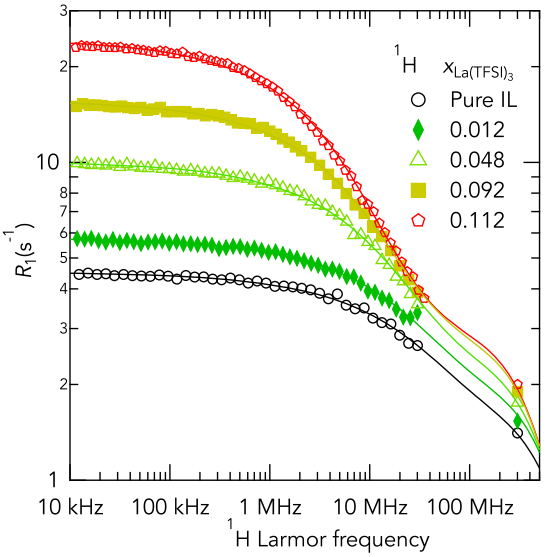


**Fig. 8.** Dispersion of the $^1$H longitudinal relaxation rate $R_1$ vs Larmor frequency of $La^{3+}$ ion solutions in [Chol][TFSI].

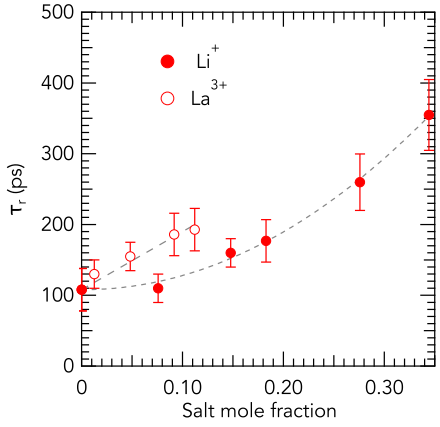


**Fig. 9.** Rotational correlation time for cholinium in the $Li^+$ and $La^{3+}$ solutions. The lines are guides for the eye.

the existence of a similar change in lanthanum system. The NMR relaxation data provide crucial insight into this phenomenon, as important changes are observed in the relaxation of the nuclei ($^{19}$F and $^7$Li) before the inversion of the long-range translational diffusion of the ions (inorganic cation/TFSI) is clearly visible. The picture of the scene, that can be built thanks to diffusion and NMR relaxation rates, is that the addition of inorganic salt in ionic liquids yields to the progressive formation of a labile network, in which the inorganic cation becomes able to move by jumping from one solvation cage formed by TFSI to another.

The combination of investigation methods used in the present study gives access to the details of the dynamics of all the species and is readily transferable to other systems of interests, e.g. energy storage systems. The practical requirements on electrolytes for supercapacitors and batteries are similar with the critical issue of the fast transport of charge carriers (Lewandowski and Świderska Mocek, 2009; Watanabe et al., 2017; Zhou et al., 2023). Consequently, the current approach might shed a new light on the solutions envisaged so far: addition of a low viscosity molecular solvent, use of a porous system to alleviate the structuring effect of the dissolved $Li^+$ ions or the addition of polar groups on the cation of the IL to gain fluidity.

## CRediT authorship contribution statement

**Ousmane Karé:** Investigation, Resources. **Antonio De Souza Braga Neto:** Investigation, Resources, Visualization, Writing – original draft. **Baptiste Rigaud:** Investigation. **Quentin Berrod:** Supervision, Writing – review & editing. **Sandrine Lyonnard:** Funding acquisition, Project administration, Supervision. **Clément Cousin:** Investigation, Resources. **Juliette Sirieix-Plénet:** Conceptualization, Funding acquisition, Project administration, Resources, Supervision, Writing – original draft. **Anne-Laure Rollet:** Conceptualization, Formal analysis, Project administration, Supervision, Visualization, Writing – original draft, Writing – review & editing. **Guillaume Mériguet:** Conceptualization, Formal analysis, Funding acquisition, Project administration, Visualization, Writing – original draft, Writing – review & editing.

## Declaration of competing interest

The authors declare that they have no known competing financial interests or personal relationships that could have appeared to influence the work reported in this paper.

## Data availability

Data will be made available on request.

## Acknowledgements

This work was partly supported by a public grant overseen by the French National Research Agency (ANR) (No. ANR-19-CE06-0025 MoveYourIon) and doctoral scholarships from Sorbonne University.

The authors are indebted to the NMR Platform and RELAXOME platform of Sorbonne University. The NMR spectrometers and relaxometers were funded by Sorbonne University, CNRS and Région Île de France, and is part of the Federation of Chemistry and Materials of Paris-Centre (FCMat).

## Appendix A. Supplementary material

Supplementary material related to this article can be found online at https://doi.org/10.1016/j.jil.2024.100087.

## References

Abragam, A., 1961. The Principles of Nuclear Magnetism. International Series of Monograph on Physics. Oxford University Press, Oxford.

Aguilera, L., Völkner, J., Labrador, A., Matic, A., 2015. The effect of lithium salt doping on the nanostructure of ionic liquids. Phys. Chem. Chem. Phys. 17, 27082–27087. https://doi.org/10.1039/C5CP03825A.

Anoardo, E., Galli, G., Ferrante, G., 2001. Fast-field-cycling NMR: applications and instrumentation. Appl. Magn. Reson. 20, 365–404. https://doi.org/10.1007/BF03162287.

Anouti, M., Porion, P., Brigouleix, C., Galiano, H., Lemordant, D., 2010. Transport properties in two pyrrolidinium-based protic ionic liquids as determined by conductivity, viscosity and nmr self-diffusion measurements. Fluid Phase Equilib. 299, 229–237. https://doi.org/10.1016/j.fluid.2010.09.035.

Ayant, Y., Belorizky, E., Aluzon, J., Gallice, J., 1975. Calcul des densités spectrales résultant d'un mouvement aléatoire de translation en relaxation par interaction dipolaire magnétique dans les liquides. J. Phys. France 36, 991–1004. https://doi.org/10.1051/jphys:019750036010099100.

Becher, M., Lichtinger, A., Minikejew, R., Vogel, M., Rössler, E.A., 2022. NMR relaxometry accessing the relaxation spectrum in molecular glass formers. Int. J. Mol. Sci. 23. https://doi.org/10.3390/ijms23095118.

Beckmann, J.B.B., Rauber, D., Philippi, F., Goloviznina, K., Ward-Williams, J.A., Sederman, A.J., Mantle, M.D., Pádua, A., Kay, C.W.M., Welton, T., Gladden, L.F., 2022. Molecular dynamics of ionic liquids from fast-field cycling NMR and molecular dynamics simulations. J. Phys. Chem. B 126, 7143–7158. https://doi.org/10.1021/acs.jpcb.2c01372.

Berrod, Q., Ferdeghini, F., Zanotti, J.-M., Judeinstein, P., Lairez, D., García Sakai, V., Czakkel, O., Fouquet, P., Constantin, D., 2017. Ionic liquids: evidence of the viscosity scale-dependence. Sci. Rep. 7, 2241.

Bloembergen, N., Purcell, E.E., Pound, R.R., 1948. Relaxation effects in nuclear magnetic resonance absorption. Phys. Rev. 73, 679–712. https://doi.org/10.1103/PhysRev.73.679.

Borodin, O., Smith, G.D., Henderson, W., 2006. Li+ cation environment, transport, and mechanical properties of the litfsi doped n-methyl-n-alkylpyrrolidinium+tfsi- ionic liquids. J. Phys. Chem. B 110, 16879–16886. https://doi.org/10.1021/jp061930t.

Callaghan, P.T., 2014. Translational Dynamics and Magnetic Resonance. Oxford University Press.

Carignani, E., Forte, C., Juszyńska-Gałązka, E., Gałązka, M., Massalska-Arodź, M., Geppi, M., Calucci, L., 2018. Dynamics of two glass forming monohydroxy alcohols by field cycling $^{1}$H NMR relaxometry. J. Mol. Liq. 269, 847–854. https://doi.org/10.1016/j.molliq.2018.08.112.

Castriota, M., Caruso, T., Agostino, R.G., Cazzanelli, E., Henderson, W.A., Passerini, S., 2005. Raman investigation of the ionic liquid n-methyl-n-propylpyrrolidinium bis(trifluoromethanesulfonyl)imide and its mixture with $LiN(SO_2CF_3)_2$. J. Phys. Chem. A 109, 92–96. https://doi.org/10.1021/jp046030w.

Dai, S., Ju, Y.H., Barnes, C.E., 1999. Solvent extraction of strontium nitrate by a crown ether using room-temperature ionic liquids. J. Chem. Soc., Dalton Trans., 1201–1202. https://doi.org/10.1039/A809672D.

Dokko, K., Watanabe, D., Ugata, Y., Thomas, M.L., Tsuzuki, S., Shinoda, W., Hashimoto, K., Ueno, K., Umebayashi, Y., Watanabe, M., 2018. Direct evidence for Li ion hopping conduction in highly concentrated sulfolane-based liquid electrolytes. J. Phys. Chem. B 122, 10736–10745. https://doi.org/10.1021/acs.jpcb.8b09439.

Driver, G.W., Huang, Y., Laaksonen, A., Sparrman, T., Wang, Y.-L., Westlund, P.-O., 2017. Correlated/non-correlated ion dynamics of charge-neutral ion couples: the origin of ionicity in ionic liquids. Phys. Chem. Chem. Phys. 19, 4975–4988. https://doi.org/10.1039/C6CP05801A.

Ferdeghini, F., Berrod, Q., Zanotti, J.-M., Judeinstein, P., Sakai, V.G., Czakkel, O., Fouquet, P., Constantin, D., 2017. Nanostructuration of ionic liquids: impact on the cation mobility. A multi-scale study. Nanoscale 9, 1901–1908.

Fraenza, C.C., Greenbaum, S.G., 2022. Broadband NMR relaxometry of electrolytes for energy storage. Chem. Phys. Rev. 3, 011307. https://doi.org/10.1063/5.0076580.

Fujara, F., Kruk, D., Lips, O., Privalov, A., Sinitsyn, V., Stork, H., 2008. Fluorine dynamics in $LaF_3$-type fast ionic conductors — combined results of nmr and conductivity techniques. Solid State Ion. 179, 2350–2357. https://doi.org/10.1016/j.ssi.2008.10.003.

Gerig, J., 1989. Fluorine nuclear magnetic resonance of fluorinated ligands. In: Methods Enzymol., vol. 177, pp. 3–23.

Gerig, J.T., Loehr, D.T., Luk, K.F., Roe, D.C., 1979. Fluorine nuclear relaxation studies of p-trifluoromethylbenzenesulfonyl-$\alpha$-chymotrypsin. J. Am. Chem. Soc. 101, 7482–7487. https://doi.org/10.1021/ja00519a006.

Greer, A.J., Jacquemin, J., Hardacre, C., 2020. Industrial applications of ionic liquids. Molecules 25. https://doi.org/10.3390/molecules25215207. https://www.mdpi.com/1420-3049/25/21/5207.

Haskins, J.B., Bennett, W.R., Wu, J.J., Hernández, D.M., Borodin, O., Monk, J.D., Bauschlicher, C.W.J., Lawson, J.W., 2014. Computational and experimental investigation of Li-doped ionic liquid electrolytes: [pyr14][tfsi], [pyr13][fsi], and [emim][bf4]. J. Phys. Chem. B 118, 11295–11309. https://doi.org/10.1021/jp5061705.

Hayamizu, K., Aihara, Y., Nakagawa, H., Nukuda, T., Price, W.S., 2004. Ionic conduction and ion diffusion in binary room-temperature ionic liquids composed of [emim][$BF_4$] and $LiBF_4$. J. Phys. Chem. B 108, 19527–19532. https://doi.org/10.1021/jp0476601.

Hayamizu, K., Tsuzuki, S., Seki, S., Ohno, Y., Miyashiro, H., Kobayashi, Y., 2008. Quaternary ammonium room-temperature ionic liquid including an oxygen atom in side chain/lithium salt binary electrolytes: Ionic conductivity and $^{1}$H, $^{7}$Li, and $^{19}$F NMR studies on diffusion coefficients and local motions. J. Phys. Chem. B 112, 1189–1197. https://doi.org/10.1021/jp077714h.

Hayes, R., Warr, G.G., Atkin, R., 2015. Structure and nanostructure in ionic liquids. Chem. Rev. 115, 6357–6426.

Honegger, P., Overbeck, V., Strate, A., Appelhagen, A., Sappl, M., Heid, E., Schröder, C., Ludwig, R., Steinhauser, O., 2020. Understanding the nature of nuclear magnetic resonance relaxation by means of fast-field-cycling relaxometry and molecular dynamics simulations—the validity of relaxation models. J. Phys. Chem. Lett. 11, 2165–2170. https://doi.org/10.1021/acs.jpclett.0c00087.

Huang, Q., Lourenço, T.C., Costa, L.T., Zhang, Y., Maginn, E.J., Gurkan, B., 2019. Solvation structure and dynamics of Li+ in ternary ionic liquid–lithium salt electrolytes. J. Phys. Chem. B 123, 516–527. https://doi.org/10.1021/acs.jpcb.8b08859.

Hwang, L.-P., Freed, J.H., 1975. Dynamic effects of pair correlation functions on spin relaxation by translational diffusion in liquids. J. Chem. Phys. 63, 4017–4025. https://doi.org/10.1063/1.431841.

Jayakody, N.K., Fraenza, C.C., Greenbaum, S.G., Ashby, D., Dunn, B.S., 2020. NMR relaxometry and diffusometry analysis of dynamics in ionic liquids and ionogels for use in lithium-ion batteries. J. Phys. Chem. B 124, 6843–6856. https://doi.org/10.1021/acs.jpcb.0c02755.

Johnson, C., 1999. Diffusion ordered nuclear magnetic resonance spectroscopy: principles and applications. Prog. Nucl. Magn. Reson. Spectrosc. 34, 203–256. https://doi.org/10.1016/S0079-6565(99)00003-5.

Judeinstein, P., Zeghal, M., Constantin, D., Iojoiu, C., Coasne, B., 2021. Interplay of structure and dynamics in lithium/ionic liquid electrolytes: experiment and molecular simulation. J. Phys. Chem. B 125, 1618–1631. https://doi.org/10.1021/acs.jpcb.0c09597.

Khudozhitkov, A.E., Paschek, D., Stepanov, A.G., Kolokolov, D.I., Ludwig, R., 2023. How like-charge attraction influences the mobility of cations in hydroxyl-functionalized ionic liquids. Chem. Phys. Lett. 14, 4019–4025. https://doi.org/10.1021/acs.jpclett.3c00463.

Kimmich, R., 1997. NMR Tomography, Diffusometry, Relaxometry. Springer Berlin Heidelberg.

Kimmich, R., 2012. Principles of Soft-Matter Dynamics. Springer, Dordrecht.

Kimmich, R. (Ed.), 2019. Field-Cycling NMR Relaxometry, New Developments in NMR. The Royal Society of Chemistry.

Korb, J.-P., 2018. Multiscale nuclear magnetic relaxation dispersion of complex liquids in bulk and confinement. Prog. Nucl. Magn. Reson. Spectrosc. 104, 12–55. https://doi.org/10.1016/j.pnmrs.2017.11.001.

Kowalewski, J., Mäler, L., 2006. Relaxation through dipolar interactions. In: Nuclear Spin Relaxation in Liquids: Theory, Experiments, and Applications. Taylor & Francis, pp. 40–63.

Kruk, D., Herrmann, A., Rössler, E.a., 2012. Field-cycling NMR relaxometry of viscous liquids and polymers. Prog. Nucl. Magn. Reson. Spectrosc. 63, 33–64. https://doi.org/10.1016/j.pnmrs.2011.08.001.

Kruk, D., Meier, R., Rachocki, A., Korpała, A., Singh, R.K., Rössler, E.A., 2014. Determining diffusion coefficients of ionic liquids by means of field cycling nuclear magnetic resonance relaxometry. J. Chem. Phys. 140, 244509. https://doi.org/10.1063/1.4882064.

Kruk, D., Wojciechowski, M., Brym, S., Singh, R.K., 2016. Dynamics of ionic liquids in bulk and in confinement by means of $^{1}$H NMR relaxometry – BMIM-$OcSO_4$ in an $SiO_2$ matrix as an example. Phys. Chem. Chem. Phys. 18, 23184–23194. https://doi.org/10.1039/C6CP02377K.

Kruk, D., Wojciechowski, M., Florek-Wojciechowska, M., Singh, R.K., 2020. Dynamics of ionic liquids in confinement by means of NMR relaxometry—EMIM-FSI in a

silica matrix as an example. Materials (Basel) 13, 4351. https://doi.org/10.3390/ma13194351.

Kubota, K., Siroma, Z., Sano, H., Kuwabata, S., Matsumoto, H., 2018. Diffusion of lithium cation in low-melting lithium Molten salts. J. Phys. Chem. C 122, 4144–4149. https://doi.org/10.1021/acs.jpcc.7b11281.

Lassègues, J.-C., Grondin, J., Talaga, D., 2006. Lithium solvation in bis(trifluoromethanesulfonyl)imide-based ionic liquids. Phys. Chem. Chem. Phys. 8, 5629–5632. https://doi.org/10.1039/B615127B.

Lassègues, J.C., Grondin, J., Aupetit, C., Johansson, P., 2009. Spectroscopic identification of the lithium ion transporting species in LiTFSI-doped ionic liquids. J. Phys. Chem. A 113, 305–314. https://doi.org/10.1021/jp806124w.

Le, M.L.P., Alloin, F., Strobel, P., Leprêtre, J.-C., Pérez del Valle, C., Judeinstein, P., 2010. Structure-properties relationships of lithium electrolytes based on ionic liquid. J. Phys. Chem. B 114, 894–903. https://doi.org/10.1021/jp9098842.

Lesch, V., Jeremias, S., Moretti, A., Passerini, S., Heuer, A., Borodin, O., 2014. A combined theoretical and experimental study of the influence of different anion ratios on lithium ion dynamics in ionic liquids. J. Phys. Chem. B 118, 7367–7375. https://doi.org/10.1021/jp501075g.

Lewandowski, A., Świderska Mocek, A., 2009. Ionic liquids as electrolytes for Li-ion batteries—an overview of electrochemical studies. J. Power Sources 194, 601–609. https://doi.org/10.1016/j.jpowsour.2009.06.089.

Li, Z., Smith, G.D., Bedrov, D., 2012. $Li^+$ solvation and transport properties in ionic liquid/lithium salt mixtures: a molecular dynamics simulation study. J. Phys. Chem. B 116, 12801–12809. https://doi.org/10.1021/jp3052246.

Liu, T., Liu, Z., Kim, G., Frith, J.T., Garcia-Araez, N., Grey, C.P., 2017. Understanding LiOH chemistry in a ruthenium-catalyzed Li–$O_2$ battery. Angew. Chem. Int. Ed. 56, 16057–16062. https://doi.org/10.1002/anie.201709886.

Monteiro, M.J., Bazito, F.F.C., Siqueira, L.J.A., Ribeiro, M.C.C., Torresi, R.M., 2008. Transport coefficients, Raman spectroscopy, and computer simulation of lithium salt solutions in an ionic liquid. J. Phys. Chem. B 112, 2102–2109. https://doi.org/10.1021/jp077026y.

Monteiro, M.J., Camilo, F.F., Ribeiro, M.C.C., Torresi, R.M., 2010. Ether-bond-containing ionic liquids and the relevance of the ether bond position to transport properties. J. Phys. Chem. B 114, 12488–12494. https://doi.org/10.1021/jp104419k.

Ngo, H.P.K., Planes, E., Iojoiu, C., Soudant, P., Rollet, A.-L., Judeinstein, P., 2022. Transport properties of alkali/alkaline Earth cations in ionic-liquid based electrolytes. J. Ionic Liq. 2, 100044. https://doi.org/10.1016/j.jil.2022.100044.

Nicotera, I., Oliviero, C., Henderson, W.A., Appetecchi, G.B., Passerini, S., 2005. NMR investigation of ionic liquid-LiX mixtures: pyrrolidinium cations and $TFSI^-$ anions. J. Phys. Chem. B 109, 22814–22819. https://doi.org/10.1021/jp053799f.

Niemann, T., Neumann, J., Stange, P., Gärtner, S., Youngs, T.G.A., Paschek, D., Warr, G.G., Atkin, R., Ludwig, R., 2019. The double-faced nature of hydrogen bonding in hydroxy-functionalized ionic liquids shown by neutron diffraction and molecular dynamics simulations. Angew. Chem. Int. Ed. 58, 12887–12892. https://doi.org/10.1002/anie.201904712.

Nockemann, P., Binnemans, K., Thijs, B., Parac-Vogt, T.N., Merz, K., Mudring, A.-V., Menon, P.C., Rajesh, R.N., Cordoyiannis, G., Thoen, J., Leys, J., Glorieux, C., 2009. Temperature-driven mixing-demixing behavior of binary mixtures of the ionic liquid choline bis(trifluoromethylsulfonyl)imide and water. J. Phys. Chem. B 113, 1429–1437.

Okamura, H., Hirayama, N., 2021. Recent progress in ionic liquid extraction for the separation of rare Earth elements. Anal. Sci. 37, 119–130. https://doi.org/10.2116/analsci.20SAR11.

Ordikhani-Seyedlar, A., Stapf, S., Mattea, C., 2015. Dynamics of the ionic liquid 1-butyl-3-methylimidazolium bis(trifluoromethylsulphonyl)imide studied by nuclear magnetic resonance dispersion and diffusion. Phys. Chem. Chem. Phys. 17, 1653–1659. https://doi.org/10.1039/C4CP04178J.

Overbeck, V., Golub, B., Schröder, H., Appelhagen, A., Paschek, D., Neymeyr, K., Ludwig, R., 2020. Probing relaxation models by means of fast field-cycling relaxometry, NMR spectroscopy and molecular dynamics simulations: detailed insight into the translational and rotational dynamics of a protic ionic liquid. J. Mol. Liq. 319, 114207. https://doi.org/10.1016/j.molliq.2020.114207.

Overbeck, V., Appelhagen, A., Rößler, R., Niemann, T., Ludwig, R., 2021. Rotational correlation times, diffusion coefficients and quadrupolar peaks of the protic ionic liquid ethylammonium nitrate by means of $^1H$ fast field cycling NMR relaxometry. J. Mol. Liq. 322, 114983. https://doi.org/10.1016/j.molliq.2020.114983.

Price, W.S., 2009. Diffusion and Its Measurement, Cambridge Molecular Science. Cambridge University Press, pp. 1–68.

Rollet, A.-L., Salanne, M., 2011. Studies of the local structures of Molten metal halides. Annu. Rep. Prog. Chem., Sect. C, Phys. Chem. 107, 88–123. https://doi.org/10.1039/C1PC90003J.

Rollet, A.-L., Simonin, J.-P., Turq, P., Gebel, G., Kahn, R., Vandais, A., Noël, J.-P., Malveau, C., Canet, D., 2001. Self-diffusion of ions at different time scales in a porous and charged medium: the Nafion membrane. J. Phys. Chem. B 105, 4503–4509. https://doi.org/10.1021/jp0023462.

Rollet, A.-L., Porion, P., Vaultier, M., Billard, I., Deschamps, M., Bessada, C., Jouvensal, L., 2007. Anomalous diffusion of water in [BMIM][TFSI] room-temperature ionic liquid. J. Phys. Chem. B 111, 11888–11891. https://doi.org/10.1021/jp075378z.

Rollet, A.-L., Godier, S., Bessada, C., 2008. High temperature nmr study of the local structure of Molten $LaF_3$–AF (A = Li, Na, K and Rb) mixtures. Phys. Chem. Chem. Phys. 10, 3222–3228. https://doi.org/10.1039/B719158H.

Rollet, A.-L., Sarou-Kanian, V., Bessada, C., 2009. Measuring self-diffusion coefficients up to 1500 K: a powerful tool to investigate the dynamics and the local structure of inorganic melts. Inorg. Chem. 48, 10972–10975. https://doi.org/10.1021/ic9010086.

Saito, Y., Umecky, T., Niwa, J., Sakai, T., Maeda, S., 2007. Existing condition and migration property of ions in lithium electrolytes with ionic liquid solvent. J. Phys. Chem. B 111, 11794–11802. https://doi.org/10.1021/jp072998r.

Solano, C.J.F., Jeremias, S., Paillard, E., Beljonne, D., Lazzaroni, R., 2013. A joint theoretical/experimental study of the structure, dynamics, and $Li^+$ transport in bis([tri]fluoro[methane]sulfonyl)imide [t]FSI-based ionic liquids. J. Chem. Phys. 139, 034502. https://doi.org/10.1063/1.4813413.

Srour, H., Traïkia, M., Fenet, B., Rouault, H., Costa Gomes, M.F., Santini, C.C., Husson, P., 2015. Effect of nitrile-functionalization of imidazolium-based ionic liquids on their transport properties, both pure and mixed with lithium salts. J. Solution Chem. 44, 495–510. https://doi.org/10.1007/s10953-014-0280-2.

Strate, A., Niemann, T., Michalik, D., Ludwig, R., 2017. When like charged ions attract in ionic liquids: controlling the formation of cationic clusters by the interaction strength of the counterions. Angew. Chem. Int. Ed. 56, 496–500. https://doi.org/10.1002/anie.201609799.

Taige, M., Hilbert, D., Schubert, T.J.S., 2012. Mixtures of ionic liquids as possible electrolytes for lithium ion batteries. Z. Phys. Chem. 226, 129–139. https://doi.org/10.1524/zpch.2012.0161.

Tong, J., Wu, S., von Solms, N., Liang, X., Huo, F., Zhou, Q., He, H., Zhang, S., 2020. The effect of concentration of lithium salt on the structural and transport properties of ionic liquid-based electrolytes. Front. Chem. 7. https://doi.org/10.3389/fchem.2019.00945.

Tsuzuki, S., Hayamizu, K., Seki, S., 2010. Origin of the low-viscosity of [emim][$(FSO_2)_2$N] ionic liquid and its lithium salt mixture: experimental and theoretical study of self-diffusion coefficients, conductivities, and intermolecular interactions. J. Phys. Chem. B 114, 16329–16336. https://doi.org/10.1021/jp106870v.

Umebayashi, Y., Mori, S., Fujii, K., Tsuzuki, S., Seki, S., Hayamizu, K., Ishiguro, S.-i., 2010. Raman spectroscopic studies and ab initio calculations on conformational isomerism of 1-butyl-3-methylimidazolium bis-(trifluoromethanesulfonyl)amide solvated to a lithium ion in ionic liquids: effects of the second solvation sphere of the lithium ion. J. Phys. Chem. B 114, 6513–6521. https://doi.org/10.1021/jp100898h.

Umebayashi, Y., Hamano, H., Seki, S., Minofar, B., Fujii, K., Hayamizu, K., Tsuzuki, S., Kameda, Y., Kohara, S., Watanabe, M., 2011. Liquid structure of and $Li^+$ ion solvation in bis(trifluoromethanesulfonyl)amide based ionic liquids composed of 1-ethyl-3-methylimidazolium and n-methyl-n-propylpyrrolidinium cations. J. Phys. Chem. B 115, 12179–12191. https://doi.org/10.1021/jp2072827.

Vicent-Luna, J.M., Azaceta, E., Hamad, S., Ortiz-Roldán, J.M., Tena-Zaera, R., Calero, S., Anta, J.A., 2018. Molecular dynamics analysis of charge transport in ionic-liquid electrolytes containing added salt with mono, di, and trivalent metal cations. ChemPhysChem 19, 1665–1673. https://doi.org/10.1002/cphc.201701326.

Watanabe, M., Thomas, M.L., Zhang, S., Ueno, K., Yasuda, T., Dokko, K., 2017. Application of ionic liquids to energy storage and conversion materials and devices. Chem. Rev. 117, 7190–7239. https://doi.org/10.1021/acs.chemrev.6b00504.

Wencka, M., Apih, T., Korošec, R.C., Jenczyk, J., Jarek, M., Szutkowski, K., Jurga, S., Dolinšek, J., 2017. Molecular dynamics of 1-ethyl-3-methylimidazolium triflate ionic liquid studied by $^1H$ and $^{19}F$ nuclear magnetic resonances. Phys. Chem. Chem. Phys. 19, 15368–15376. https://doi.org/10.1039/c7cp01045a.

Wu, D., Chen, A., Johnson, C., 1995. An improved diffusion-ordered spectroscopy experiment incorporating bipolar-gradient pulses. J. Magn. Reson., Ser. A 115, 260–264. https://doi.org/10.1006/jmra.1995.1176.

Wu, T.-Y., Hao, L., Kuo, C.-W., Lin, Y.-C., Su, S.-G., Kuo, P.-L., Sun, I.-W., 2012. Ionic conductivity and diffusion in lithium tetrafluoroborate-doped 1-methyl-3-pentylimidazolium tetrafluoroborate ionic liquid. Int. J. Electrochem. Sci. 7, 2047–2064. https://doi.org/10.1016/S1452-3981(23)13862-4.

Xu, X., Su, L., Lu, F., Yin, Z., Gao, Y., Zheng, L., Gao, X., 2022. Unraveling anion effect on lithium ion dynamics and interactions in concentrated ionic liquid electrolyte. J. Mol. Liq. 361, 119629. https://doi.org/10.1016/j.molliq.2022.119629.

Yang, M.Y., Merinov, B.V., Zybin, S.V., Goddard III, W.A., Mok, E.K., Hah, H.J., Han, H.E., Choi, Y.C., Kim, S.H., 2022. Transport properties of imidazolium based ionic liquid electrolytes from molecular dynamics simulations. Electrochem. Sci. Adv. 2, e2100007. https://doi.org/10.1002/elsa.202100007.

Zhou, T., Gui, C., Sun, L., Hu, Y., Lyu, H., Wang, Z., Song, Z., Yu, G., 2023. Energy applications of ionic liquids: recent developments and future prospects. Chem. Rev. 123, 12170–12253. https://doi.org/10.1021/acs.chemrev.3c00391.